On the origin of the sigmoid shape in the UO$_2$ oxidation weight gain curves

L. Quémard [a], L. Desgranges [a,*], V. Bouineau [a], M. Pijolat [b], G. Baldinozzi [c],
N. Millot [d], J.C. Nièpce [d], A. Poulesquen [e]

[a] CEA Cadarache, DEN/DEC/SA3C/L2EC Bât. 316, 13108 St. Paul-lez-Durance, France
[b] LPMG, Ecole Nationale Supérieure des Mines de St-Etienne, Centre SPIN, Equipe PROCESS, 158, Cours Fauriel, 42023 St-Etienne CEDEX 2, France
[c] SPMS, UMR 8580 CNRS-Ecole Centrale Paris, Grande Voie des Vignes, 92295 Châtenay-Malabry, France
[d] ICB, Equipe MANAPI, UMR 5209 CNRS-Université de Bourgogne, 9 Av. Alain Savary, BP 47870, 21078 Dijon, France
[e] CEA Saclay, DEN/DPC/SECR/L3MR, Bat. 450, 91191 Gif-sur-Yvette, France

Abstract

Cracking and spalling are known to occur during the oxidation of UO$_2$. However, these phenomena are not considered by the existing kinetic models of the oxidation of UO$_2$ into U$_3$O$_8$. In this study the oxidation of UO$_2$ samples of various sizes from the single crystal to nanopowders, has been followed by isothermal and isobaric thermogravimetry, environmental scanning electron microscopy and in situ X-ray diffraction at temperatures ranging from 250 to 370 °C in air. It has been shown that cracking occurs once a critical layer thickness of intermediate oxide has been reached, which corresponds to the beginning of the sigmoid kinetic curve. Cracking contribution to the sigmoid kinetic curve is then discussed as a function of temperature, and on the basis of nucleation and growth processes.
© 2009 Elsevier Ltd. All rights reserved.

Keywords: UO$_2$; Nuclear applications; Electron microscopy; X-ray methods

1. Introduction

The stepwise oxidation of UO$_2$ in air to form U$_3$O$_7$ and U$_3$O$_8$ has been studied extensively for about 50 years, because of its relevance to the dry storage and the ultimate disposal of used nuclear fuel, as well as UO$_2$ powder storage and some fuel-recycling processes (see [1] for a comprehensive review). The oxidation of UO$_2$ powders is usually partitioned in two stages: the first one is associated to a pseudo-parabolic weight gain curve while the second one is associated to a sigmoid weight gain curve. The pseudo-parabolic curve, attributed the formation of U$_4$O$_9$ and U$_3$O$_7$ on UO$_2$ powders, indicates a diffusion-controlled mechanism,[2] for the modelling of which a finite difference algorithm[3] was recently developed. The sigmoid curve is generally interpreted as the oxidation of U$_3$O$_7$ into U$_3$O$_8$ with a nucleation and growth mechanism.[4] This sigmoid curve is still a subject of debate in its quantitative interpretation. More precisely, the apparent activation energy for U$_3$O$_8$ formation deduced from the kinetic analysis of the experimental sigmoid curves, based on Avrami type laws, differs widely depending on the authors,[4] from 48 to 194 kJ mol^{-1}. This great dispersion can be reduced by considering that U$_3$O$_8$ activation energy depends on the physical state of the sample, for example powder or pellet,[5] but the physical basis for this assumption is questionable. Another interpretation was proposed considering different U$_3$O$_8$ activation energies in two temperature ranges with a change in oxidation behaviour around 300–350 °C.[6] Although this last interpretation is now widely admitted, the physical mechanisms underlying this oxidation behaviour change remain unclear.

In fact the quantitative interpretation of the sigmoid curve has to face two technical difficulties[4]:

- the sigmoid curve has to be extracted form the experimental data which also include the pseudo-parabolic curve,
- the spalling of the sample, induced by the apparition of numerous cracks, has to be taken into account.

In addition, the Avrami laws generally used for the kinetic analysis of nucleation and growth processes are not appropriate

---

in the case of solids reacting with gases for which the nuclei of the new phase necessarily appear at the surface of the initial solid phase.

In order to overcome the first difficulty McEachern et al. proposed that: "with unirradiated, sintered pellets, weight gain data can be modelled with sigmoid kinetics corresponding to the direct conversion from UO_2 to U_3O_8 since there is only a thin layer of U_3O_7 formed at the reaction interface". Valdivieso et al.[7] applied several kinetic tests in order to study UO_2 pellet oxidation at 370 °C, where McEachern's proposed conditions are verified. They showed that the oxidation kinetics can be described by a rate-limiting step of growth which does not change the over all reaction. But, thanks to a comparative study of UO_2 pellet morphology and their weight gain curves, Bae et al.[8] stated that, for pellet oxidised at 400 °C, "after incubation time, crack propagation rate could control the constant oxidation rate". Considering these two papers, the physical origin of the sigmoid curve remains unclear and controversial.

Aronson et al.[9] first proposed that the formation of U_3O_8 follows a nucleation-and-growth mechanism because of the sigmoid reaction kinetics. But no other experimental proof was given to justify this interpretation. On the other hand Lefort et al. studied the oxidation of cubic niobium in air, and modelled the sigmoid isotherm weight gain curves taking into account sample cracking.[10] In their approach, which was based on a correlation between the kinetic rate and the surface area of the sample measured after various reaction periods, cracking induces the sigmoid weight gain curves by increasing the sample reactive surface. However, in the case of UO_2 oxidation, the cracking has not been very well characterised, in particular the nature of the cracks during the reaction, the influence of the particle size on the cracking process as well as the links between the cracks and the kinetics. The goal of this paper is to improve the description of the cracking process and its links with the kinetics during UO_2 oxidation in the range 250–370 °C and for various sample sizes ranging from a single crystal to a nanopowder.

For that purpose two different experimental approaches were used to estimate the role of cracking in the kinetic rate:

- The chemical phases existing on UO_2 single crystal were characterised before and after crack formation with X-ray diffraction.
- The oxidation rate at which cracking occurs was determined by the comparison of UO_2 morphologic evolution measured by environmental scanning electron microscope (ESEM) with the corresponding weight gain curves measured by thermo gravimetric analysis (TGA). Cracking was characterised on several UO_2 samples – single crystals, pellets and powders – in the 250–370 temperature range, corresponding to the lowest and highest temperature at which cracking could be characterised with ESEM.

The influence of cracking phenomenon on the oxidation process of UO_2 will be discussed for different temperatures and different grain sizes.

2. Experimental

The UO_2 samples are micrometric and nanometric powders, single crystals and fuel pellets (Table 1). The stoichiometry of powders is close to $UO_{2.02}$ and grain size ranges from 5 to 10 μm for the micrometric powders and from 100 to 200 nm for the nanometric powder. 10 μm grain size pellets were broken to get sub-millimetre size pieces that could fit in the different experimental devices.

The TGA experiments were conducted using a thermoanalyser TG-DSC 111 (Setaram, France) in a $He/O_{2(g)}$ (80/20) gas mixture flowing at 0.03 L min^{-1} and at temperatures ranging from 250 to 330 °C. The gas mixture is introduced few minutes before the beginning of the heating. A reduction treatment is performed on the UO_2 powders before oxidation during 15 min at 550 °C in a $He/H_{2(g)}$ (96/4) gas mixture flowing at 0.03 L min^{-1} to remove the oxide layer and the adsorbed species (H_2O, OH^-, etc.).

The in situ oxidation tests were carried out using the environmental scanning electron microscope (ESEM FEG XL30, Philips) and performed at temperatures ranging from 250 to 370 °C with an oxygen residual partial pressure around 260 Pa for time durations up to 6 h.

The in situ X-ray diffraction experiments were conducted using a diffractometer developed at SPMS and equipped with a 1D detector. Monochromatic Cu-Kα X-rays (λ = 0.154056 nm) were obtained with a primary focusing Ge monochromator. A Gobel mirror (Rigaku, Japan) with an optical element made of a multi-layer coating of W/Si is used to focus and increase the intensity of the incident beam. In situ oxidations in air were performed with a high temperature furnace developed at SPMS. The full 2θ range over which data was collected was from 12° to 100°.

3. Results

3.1. In situ X-ray diffraction

The diffraction patterns were interpreted with the reported crystalline structures of uranium oxides.[1] The UO_2 starting material adopts the fluorite type lattice with a cell parameter of 0.547 nm. U_3O_7 crystalline structures are tetragonal ($a = 0.538$ nm and $c = 0.554$ nm).

U_3O_7 phase is detected after an in situ oxidation of a UO_2 single crystal at 300 °C in air for 1.5 h (Fig. 1). (1 1 1), (2 2 2) and (3 3 3) diffraction peaks of U_3O_7 (2θ = 28.6°, 59.1° and 95.4°, respectively) are detected on the (1 1 1) surface of the single crystal. This shows the preferred orientations of the oxides when grown on a UO_2 single crystal as reported by Allen and Tempest for U_3O_8.[11]

Fig. 2 shows the evolution of a (ω − 2θ) diffraction pattern of the UO_2 single crystal in situ oxidised at 300 °C in air. The X-ray diffraction maps, recorded at room temperature using a mesh of 80 × 60 points with a 4 s count time per step, represent the 2θ angle versus the ω angle. After 1.5 h oxidation, the spot corresponding to the (1 1 1) U_3O_7 diffraction plan is 10 times wider than the UO_2 spot in the ω direction. This suggests some
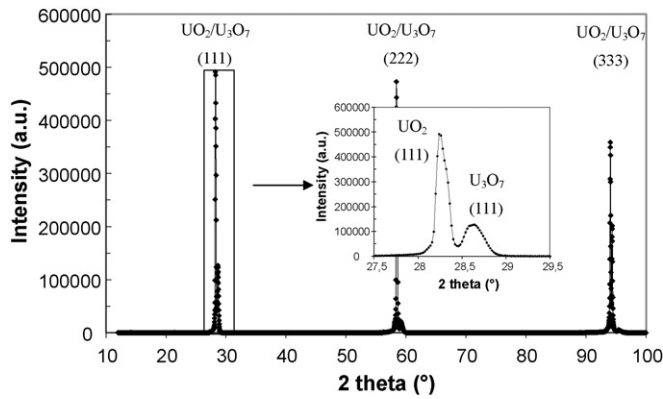
Fig. 1. In situ X-ray diffraction pattern of a (1 1 1) surface of a UO$_2$ single crystal after an oxidation at 300 °C for 1.5 h in air.

disorientation of the U$_3$O$_7$ crystallites grown on the UO$_2$ single crystal. No significant evolution occurs after 3.5 h oxidation but a splitting of UO$_2$ and U$_3$O$_7$ spots is detected after 10 h. This corresponds to a crack formation as confirmed by a post-oxidation examination of the surface using an optical microscope.

XRD results provide a rough evaluation of the U$_3$O$_7$ layer depth when the first crack was formed. The calculated attenuation length of Cu-Kα X-rays in UO$_2$ is around 800 nm at $2\theta = 28°$; it implies that the thickness of the U$_3$O$_7$ layer at which first crack occurs is lower than 1 μm.

The splitting of the (1 1 1) spot of UO$_2$ shows that this crack, appeared in the U$_3$O$_7$ layer, has propagated into the UO$_2$
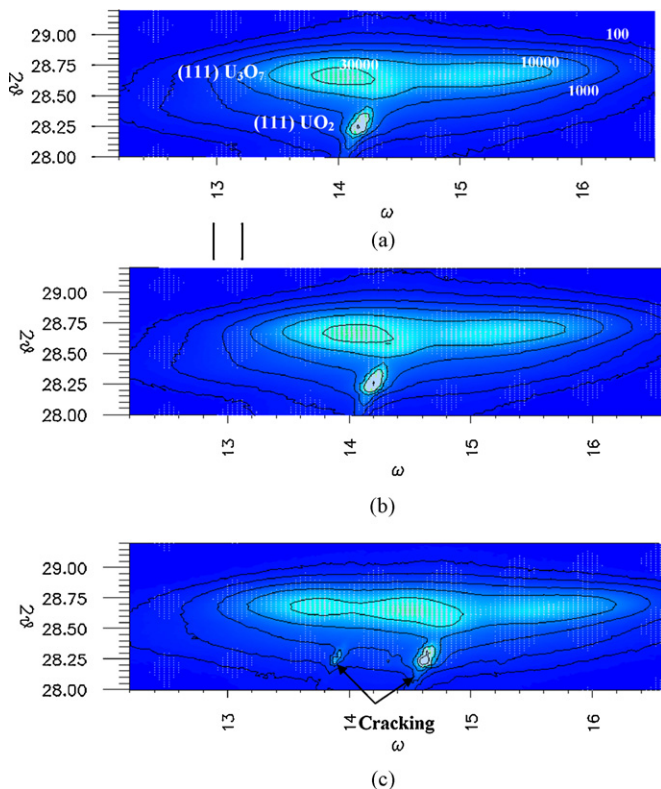

Fig. 2. X-ray diffraction maps of a (1 1 1) surface of a UO$_2$ single crystal after an in situ oxidation treatment at 300 °C in air for (a) 1.5 h, (b) 3.5 h and (c) 10 h. The intensities (a.u.) are reported close to the level lines.

substrate. Thus the cracking phenomenon induced new fresh surfaces more reactive than the initial one because of a lower oxidation rate.

3.2. Comparison between morphologic evolution and kinetic curves from weight gain

The in situ oxidation tests performed at temperatures ranging from 250 to 370 °C on the UO$_2$ single crystals, fuel pellets and micrometric powders show a continuous cracking up to grain sizes inferior to micron (Fig. 3a–i). Two types of cracking are observed. First macro-cracks occurred close to the heterogeneities of the single crystals such as angles, surface defects, etc. (Fig. 3a and b); for the fuel pellets, these macro-cracks occurred at the grain boundaries (Fig. 3e). Macro-cracking is followed by micro-cracking starting at cracked surfaces which only enhances spallation (Fig. 3c and f). Similar cracking has been observed with the 10 μm UO$_2$ grain. The final grains of U$_3$O$_8$ coming from the cracking of both single crystals and fuel pellets exhibit similar morphologies and grain sizes around 100 nm (Fig. 4a and b). Our results confirmed Bae's description for pellet fragments[8] and showed its relevance for single crystals and 10 μm grains, with intra-granular instead of inter-granular macro-cracking (cf Fig. 3). In the following, cracking analysis is focused on macro-cracking, because macro-cracking is more likely to generate reactive surfaces at the beginning of the oxidation process.

An incubation period before the first macro-cracks occur is highlighted for all the samples from ESEM experiments (Fig. 5). It appears to be dependent on the oxidation temperature and ranges from several minutes at 330 °C to several hours at 250 °C. Considering the growth of an U$_3$O$_7$ layer on UO$_2$ and assuming a plane geometry and a diffusion controlled process, the incubation period before cracking t_{crack} (s) can be related to the parabolic rate constant k (m^2 s^{-1}) considering the following equation:

$$e_{crack} = (k \cdot t_{crack})^{1/2} \qquad (1)$$

with e_{crack}: oxide layer thickness when first cracks occur (m).

Experimental values of k (m^2 s^{-1}) associated to the transformation of UO$_2$ into U$_3$O$_7$ were compiled and evaluated by McEachern,[2] who reported that the parabolic rate constant is described by the expression:

$$\ln (k) = -\frac{95700}{RT} - 17.33 \qquad (2)$$

with T: temperature (K) and $R = 8.31$ J K^{-1} mol^{-1}.

The values of e_{crack} can thus be calculated from Eqs. (1) and (2) considering the as-measured incubation periods at temperatures in the range 250–370 °C. The oxide layer thicknesses corresponding to the first cracks are very similar with an average equal to 0.4 μm; this thickness is probably related to a critical mechanical stress for the integrity of the UO$_2$ micro- or macro-crystal.

Fig. 6 shows the kinetic curves, obtained from thermogravimetric experiments, giving the effective fractional conversion (α) of UO$_2$ into U$_3$O$_8$ for single crystals and powders versus
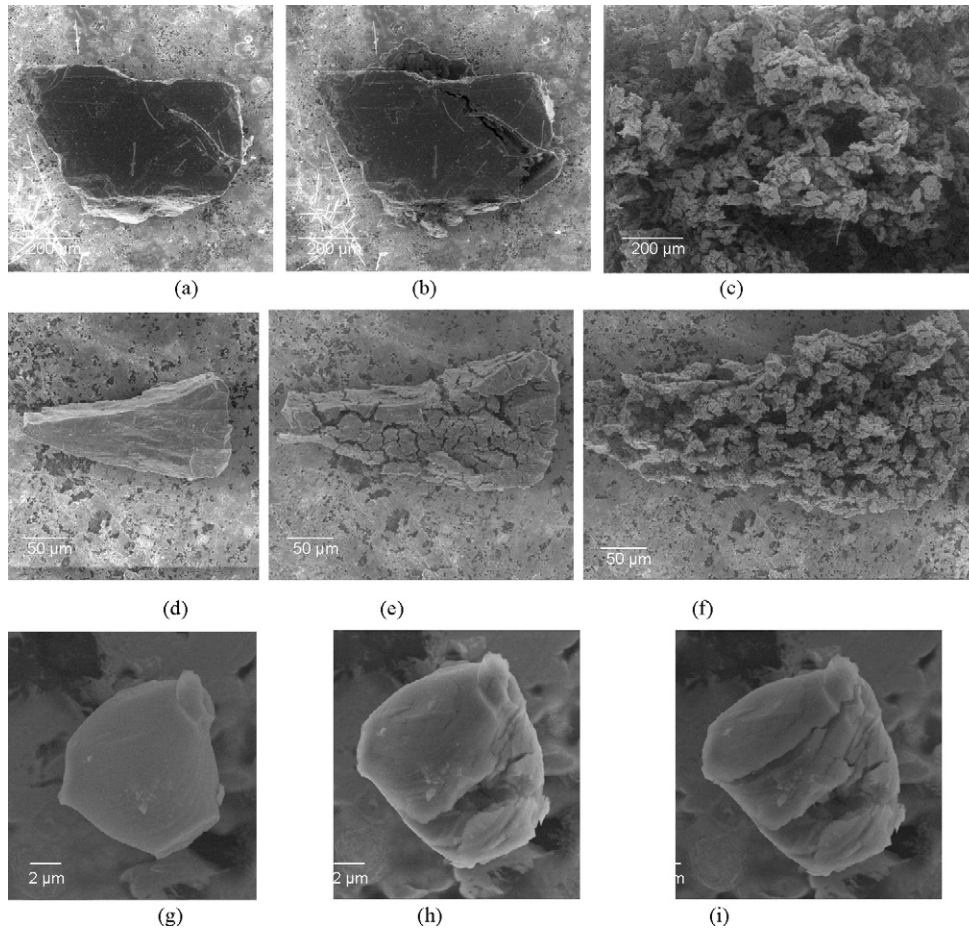
Fig. 3. ESEM micrographs showing the cracking of: a UO_2 single crystal in situ oxidised at 330 °C and $P_{O_2} = 265$ Pa: (a) initial state, (b) after 0.5 h and (c) after 5.5 h (final state). A UO_2 fuel pellet piece in situ oxidised at 330 °C and $P_{O_2} = 265$ Pa: (d) initial state, (e) after 0.5 h and (f) after 5.5 h (final state). A 10 μm UO_2 grain in situ oxidised at 330 °C and $P_{O_2} = 265$ Pa: (g) initial state, (h) after 0.5 h and (i) after 5.5 h (final state).

time at 250 °C and a partial oxygen pressure of 20 kPa. α is calculated from the weight gain $(\Delta m/m_0)_t$, using the following equation:

$$\alpha = \frac{(\Delta m/m_0)_t}{(\Delta m/m_0)_{theo}} \qquad (3)$$

with $(\Delta m/m_0)_{theo}$: theoretical weight gain corresponding to the total oxidation into U_3O_8 (3.95%).

Fig. 6 highlights the influence of grain size on the kinetic oxidation. The initial oxidation rate corresponding to the trans-

formation into U_3O_7 (up to $\alpha \cong 0.5$) increases when the grain sizes diminishes as expected for a diffusion limited regime[1]. On the contrary, it is interesting to note that the conversion rate of U_3O_7 into U_3O_8 (corresponding to a variation of α from ∼0.5 to 1) decreases with the grain size. Thus, the oxidation rate of the nanometric powder is much lower than for the micromet-ric powders and a low fractional conversion of 0.65 is reached after a long oxidation time (100 h). A post-oxidation examina-tion using SEM shows that the nanometric powder is not cracked contrarily to the other powders. On the contrary, a post-oxidation
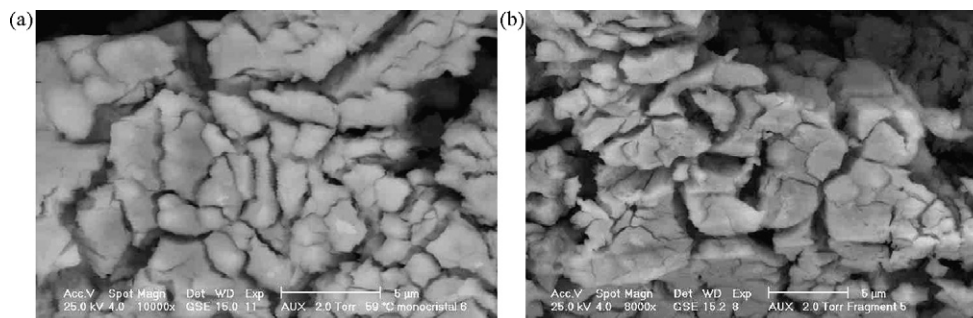

Fig. 4. ESEM micrographs showing detailed areas of the subdivided final states of (a) UO_2 single crystal and (b) UO_2 fuel pellets oxidised for 5.5 h at 330 °C and $P_{O_2} = 265$ Pa.
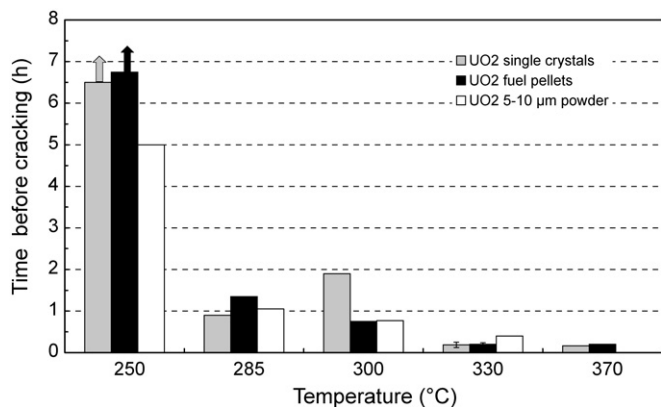
Fig. 5. Time before cracking of different samples oxidised in ESEM at different temperatures with $P_{O_2} = 265$ Pa. (At 250 °C, cracking is not observed for single crystals and fuel pellets after 6.5 and 6.75 h respectively.)

examination using SEM shows that the single crystal is already strongly subdivided for an effective fractional conversion close to 0.65. Similar results were obtained from TGA experiments performed on fuel pellets in similar oxidation conditions.

Contrarily to Bae et al. ex situ analysis,[8] spalling was not observed during the in situ ESEM experiments. With ESEM, samples did not need to be handled in order to perform observations, but they turned to powder as soon as they were removed out ESEM. This behaviour indicates that, even with heavily cracking, the cracked parts are still mechanically linked, but the cohesive forces are weak and the cracked parts turn into powder as soon as a weak stress is applied. Moreover, the macroscopic volume increase of the samples, up to 200%, is essentially due to the bulking of the solid induced by cracking compared to the swelling due to crystalline transformation into U_3O_8 which is only 36%. Consequently the change in bulk area can be used as an indicator of the number of macro-cracks created in the sample. Fig. 7 shows the macroscopic area of a piece of fuel pellet with a triangular shape (cf. Fig. 2b) measured from ESEM micrographs recorded during oxidation. Assuming the swelling is isotropic, the increase of the as-measured triangular area, called bulk area, is equal to 2/3 of the global volume expansion in a first approx-
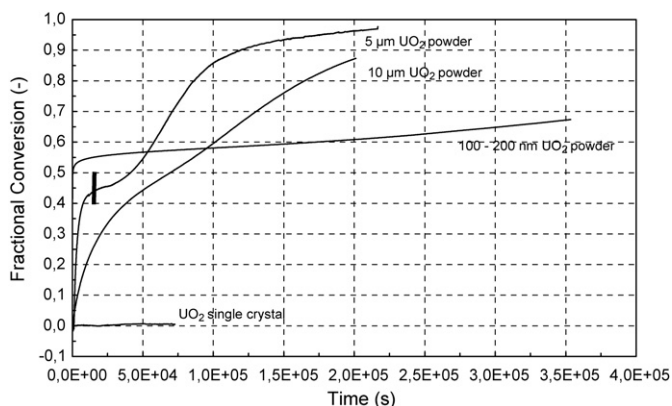
imation. Fig. 7 also shows the compared evolutions of the bulk area measured by ESEM and the oxidation kinetic curve of a fuel pellet fragment oxidised at 330 °C (similar temperature and oxygen pressure in TG and ESEM). This figure clearly evidences that kinetic oxidation continues while the bulk area is constant after 4 h oxidation.

These results evidence that macro-cracking essentially occurs at the beginning of the sigmoid curve, inducing an increase of the oxidation rate due to new reactive surfaces of UO_2. Thus the rate of U_3O_8 formation would be dependent on the rate of macro-cracking corresponding to the U_3O_7 critical oxide layer.

4. Discussion

The experimental results presented in this paper indicate that macro-cracking occurring at the beginning of the oxidation process is linked to the formation of U_3O_7. Such a process induces new reactive surfaces of UO_2. Moreover, macro-cracking seems to be only observed during the first part of the sigmoid weight gain curve. It implies that cracking should be taken into account in order to interpret sigmoid weight gain curves. Considering Rousseau et al.[12] and Valdivieso et al.[7] kinetic tests, our results also evidence that macro- and micro-cracking occur in a kinetic domain where the assumption of the rate-limiting step is verified. That is why the kinetics of the oxidation reaction will be first discussed in the framework of this assumption; the case when this assumption is not verified will be treated afterwards.

When the rate-limiting step assumption is verified, then the reaction rate can be written with by Eq. (4)[13]:

$$\frac{d\alpha}{dt} = \Phi(T, P_i) E(t) \tag{4}$$

in which Φ is a rate per unit area (mol m^{-2} s^{-1}), it depends on the nature of the rate-limiting step (diffusion, interface reaction), it is independent on time but may be a function of temperature T and partial pressures of the reacting gases P_i. $E(t)$ (m^2 mol^{-1}) is linked to the extent of the reaction zone where the rate-limiting step is located. Eq. (4) permits a more general formulation than the one usually used in solid state kinetics[14] since it does not restrict the function E to a function of α. For example, it should allow introducing the influence of cracking in the kinetic rate.

Considering UO_2 oxidation and U_3O_8 formation Valdivieso et al.[7] showed that UO_2 pellet oxidation kinetics at 370 °C is consistent with a rate-limiting step assumption of growth. By definition, the identified rate-limiting step only corresponds to an elementary step of the mechanism of growth involved in the oxidation process. In Eq. (4) this corresponds to the Φ term. Because the oxidation experiments in our study and in Valdivieso, Rousseau and Bae ones, are performed under constant thermodynamic conditions (T and PO_2), the Φ term is constant whatever the actual elementary step could be. If the E term was constant with time, then the kinetic rate would be constant and the weight gain curve would be linear with time; however, since the weight gain curve takes a sigmoid shape, the E term must not be constant and its variation with time has a sigmoid shape.

In the following the E term will be discussed qualitatively, a quantitative analysis being out of the scope of this work.

Fig. 6. Kinetic curves of different UO_2 samples oxidised at 250 °C in He/O$_2$ (80/20) gas mixture flowing at 0.03 L min^{-1}. A dashed line at $t = 2 \times 10^4$ s represents the time at which the first crack is observed with ESEM in similar conditions and with μm powder.
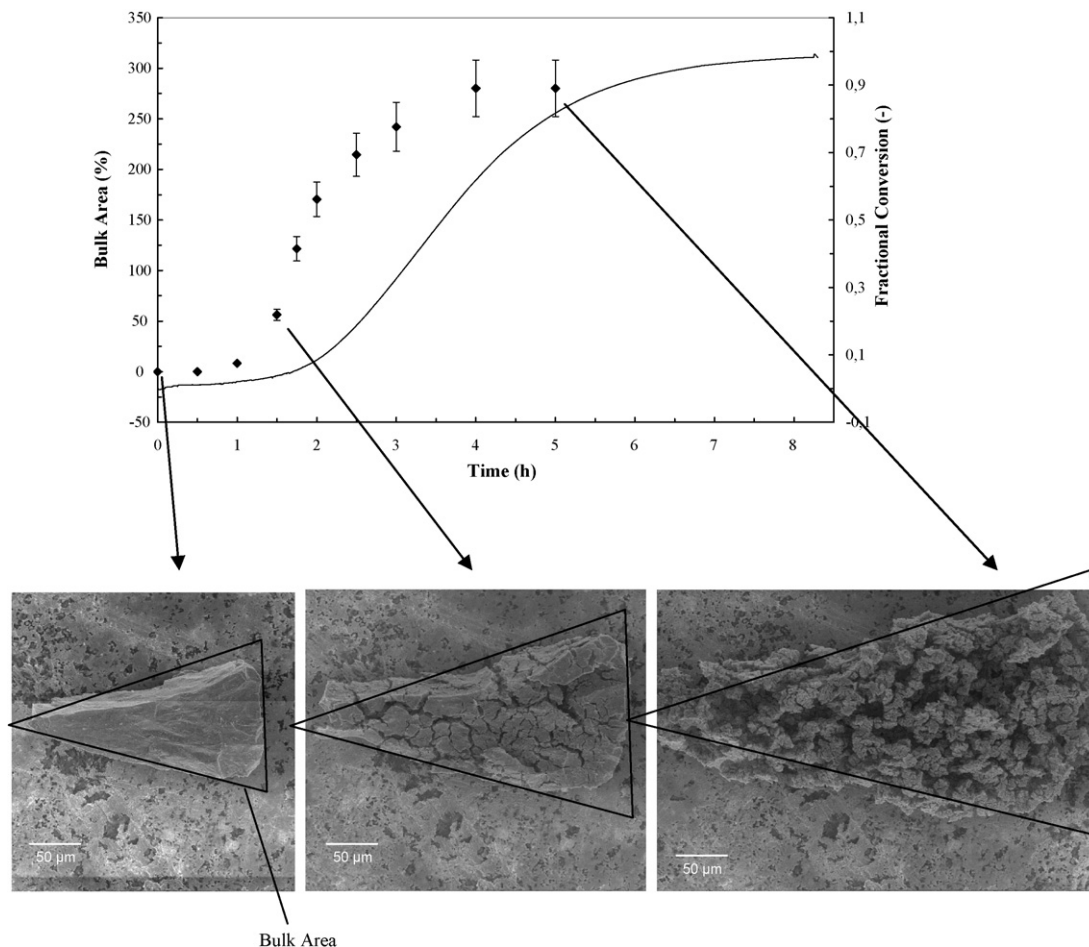
Fig. 7. Evolution of the as-measured area of a UO_2 fuel pellet oxidised at 330 °C using ESEM (experimental points) compared to the kinetic curve of a fuel pellet oxidised at 330 °C in a He/O_2 (80/20) gas mixture flowing at 0.03 L min^{-1}.

In general, for solids reacting with gases, it is possible to describe the growth mechanism as a succession of elementary steps such as adsorption (and desorption when one or several gases are produced), external interface reaction, diffusion through the produced phase, internal interface reaction. Up to now, it is not possible to decide which of these steps is the rate-limiting one. The E function associated to one of theses steps will necessarily involve the area of an "active" interface. It is thus obvious that it will depend of the surface over volume ratio (S/V) of the sample which determines, due to the steady-state conditions established in case of a rate-limiting step the oxygen flux entering in the solid. In a first approach the growth mechanism is considered to have the same time dependence at any temperature. In the following the oxidation kinetic curves for U_3O_8 formation are discussed as function of temperature in connection with the changes in S/V induced by cracking. Due to the increasing rate observed at the beginning of the kinetic curve obtained with the nanometric powder, for which no cracking was observed, the discussion will also be based on the assumption of simultaneous nucleation and growth. So at any temperature, nuclei of U_3O_8 are formed according to a nucleation mechanism which is different of that of growth; the consideration of these two processes occurring during the reaction is coherent with

the large discrepancies in the values of the apparent activation energy already mentioned.

4.1. High temperature: 370–400 °C

The morphological changes observed at 400 °C by Bae are very similar to the one we observed at lower temperature. At low temperature the cracking of the UO_2 sample was explained by the creation of a critical depth of U_3O_7 layer, but above 350 °C. U_3O_7 is not observed during oxidation of UO_2. Referring to the U–O phase diagram at thermodynamic equilibrium,[15] at 400 °C the metastable phase U_3O_7 does not exist and the UO_{2+x} compound is a mixture of UO_{2+x} and U_3O_8 phase. This implies that the oxidised layer formed on UO_2 at 400 °C would be UO_{2+x}. The UO_{2+x} phase was characterised at high temperature, and it was shown that its units cell parameter decrease with increasing x.[16] On a mechanical point of view, the formation of a UO_{2+x} layer on a UO_2 substrate creates the same stress state than the formation of U_3O_7 on UO_2 because both layers have smaller unit cell parameters that the substrate. As a consequence the interpretation proposed previously which requires a critical depth of a U_3O_7 layer for the crack formation, can be transposed to a critical layer of UO_{2+x}.

Table 1
Resume of the different oxidation conditions used in this study.

Sample	Mass (mg)	T (°C)	Gas mixture	Time (h)	Experimental
Single crystals	18–35	250–330 ± 1	He/O_2 (80/20)	8–20	TGA
	<0.3	250–370 ± 10	O_2	5–6.5	ESEM
	60	300 ± 2	air	10	XRD
Fuel pellets	<0.3	285–330 ± 1	He/O_2 (80/20)	5–14	TGA
	<0.3	250–370 ± 10	O_2	5–6.75	ESEM
Powder 10 μm	20	250 ± 1	He/O_2 (80/20)	60	TGA
	<0.3	250–330 ± 10	O_2	5–6	ESEM
Powder 5 μm	20	250 ± 1	He/O_2 (80/20)	60	TGA
Powder 200 nm	20	250 ± 1	He/O_2 (80/20)	100	TGA

At 370 °C, the weight gain curve measured during the oxidation of a UO_2 pellet has sigmoid shape with a linear part in the middle of the sigmoid.[7] The S/V ratio evolution during the oxidation and its consequences on the reaction rate can be described in four phases:

(1) at the oxidation beginning S/V is low inducing a low reaction rate,
(2) the critical thickness of the UO_{2+x} layer is reached and cracking occurs at the pellet surface. This leads to an increase in S/V which enhances the oxidation rate due to nucleation and growth of U_3O_8 at the freshly created surfaces,
(3) the reaction continues with simultaneous cracking and nucleation and growth of U_3O_8,
(4) when the pellet is totally cracked no more reactive surfaces are created. The S/V ratio is constant but the reaction continues as long as nucleation and growth proceeds until total consumption of UO_2.

4.2. Low temperature: 200–330 °C

At temperatures lower or equal to 330 °C, two main differences in the oxidation process are observed compared to the high temperature range previously described. First U_3O_7 is formed instead of UO_{2+x}, as discussed before. Then no cracking is observed to occur in the second half of the sigmoid curve (Fig. 7), which seems to be associated to a domain where the rate-limiting step is not verified.

At 250 °C, Rousseau et al.[12] performed the same kinetic tests as[7] to study the oxidation of the 5 μm UO_2 powder at 250 °C and evidenced 4 different kinetic domains. The first two domains, numbered I and II, correspond to U_4O_9 and U_3O_7 formation. The last two domains, numbered III and IV, occur in the beginning and at the end of the sigmoid curve respectively, associated to U_3O_8 formation. In domain III the assumption of a rate-limiting step is verified, while it is not in domain IV.

Domain III can be interpreted in a very similar manner to the one proposed for temperature higher that 350 °C. To interpret domain IV, a possibility could be that in addition to the nucleation and growth processes, another reaction takes place with a rate of weight increase of the same order of magnitude. This second reaction could be related to the non-stoichiometry of the U_3O_8 phase.[1] The phase formed by the previously proposed nucleation and growth mechanism could be hypo-stoichiometric U_3O_{8-z}. Its oxidation into the stoichiometric U_3O_8 phase should have a kinetic rate which increases with temperature, because of increased thermal motion. So its kinetic rate could be faster at high temperature, and of the same order of the UO_2 oxidation rate at low temperature which would explain this existence of domain IV.

At 250 °C, our results also evidenced very different weight gain curves as a function of the grain size. Because domain IV is more complex, only domain III will be discussed at the beginning of the sigmoid curve. The comparison between the grain size and the U_3O_7 critical layer thickness for crack formation can explain partly these differences. This is evidenced from Fig. 6 where the time for the first crack formation on 10 μm powder was measured at 2×10^4 s, is reported as a vertical bar. For 5 μm powders, cracking occurs at the beginning of the plateau corresponding to U_3O_7 formation as explained before. For 10 μm powders, cracking occurs before the plateau is reached. However, due to a higher initial grain size, the increase in the rate of formation of U_3O_8 will take a longer time than for lower grains (the rate, as previously discussed, is expected to be proportional to the extent of all interfaces involved in the rate-limiting step, due to the E function). For single crystals, cracking induced surface remains small compared to the powder surfaces; as a consequence no significant effect of cracking is noticed on the oxidation curves which remain nearly flat up to 7×10^4 s.

For nanometric powder, no crack formation is observed because their size is less than the U_3O_7 layer critical depth for crack formation. Only U_3O_8 formation should be observed after U_3O_7 fast formation. Nevertheless U_3O_8 formation kinetic has to be discussed because it is slower for nanometric powder than for 5–10 μm powders at the same oxidation temperature and oxygen pressure. This difference can be interpreted as a function of the chemical state of the surface on which U_3O_8 is formed, affecting its nucleation kinetic rate. For nanometric powder, U_3O_8 nuclei appear on the surface of the nanoparticles which are obviously very different to those appearing due to the cracks. It is well known that nucleation process is very dependent of the surface properties, not only the nature of the crystallographic planes, but also all the structural and chemical

defects that can be present due to the way of elaboration of the solid. For 5–10 μm powder, U_3O_8 is mostly formed on cracking induced fresh surfaces, which are not contaminated. This surface state effect on U_3O_8 formation rate is consistent with Taylor et al.,[17] who proved that surface roughness also affect U_3O_8 formation rate. In principle, U_3O_7 oxidation should also depend on surface chemical state, and hence have different oxidation kinetic on initial and cracked surfaces.

5. Conclusion

Due to a combination of in situ DRX, ESEM and TG results, it could be shown that the sigmoid shape of the weight gain curves measured during UO_2 isothermal oxidation cannot be interpreted as due to U_3O_8 nucleation and growth solely. Macro-cracking, which was shown to begin after an incubation time related to a critical layer thickness of U_3O_7 or UO_{2+x}, generates fresh reactive surfaces which are also responsible for the sigmoid shape of the kinetic curves. The relative contribution of macro-cracking and of U_3O_8 nucleation and growth to the sigmoid curve depends on temperature and sample size. As a consequence, the dispersion in the values of the apparent activation energy has to be attributed to the misinterpretation of the weight gain curves, not only because of the inappropriate Avrami's law, but also to the cracking process due to U_3O_7 or UO_{2+x} formation up to a critical layer thickness. Modelling UO_2 oxidation kinetic curves will thus require evaluating quantitatively the extent of change in the reactive surfaces due to macro-cracking as a function of time, coupled to a kinetic model of nucleation and growth of U_3O_8 from U_3O_7 or UO_{2+x} surfaces. Only the coupling of macro-cracking and U_3O_8 nucleation and growth kinetic models will give a realistic description of the UO_2 sigmoid oxidation curve and reliable kinetic constants. Work is in progress to address this point with respect to the mechanical state of the surface oxidised layer and the nucleation and growth process of U_3O_8.

Acknowledgements

References

1. McEachern, R. J. and Taylor, P., A review of the oxidation of uranium dioxide at temperature below 400 °C. *J. Nucl. Mater.*, 1998, **254**, 87–121.
2. McEachern, R. J., A review of kinetic data on the rate of U_3O_7 formation on UO_2. *J. Nucl. Mater.*, 1997, **245**, 238–247.
3. Poulesquen, A., Desgranges, L. and Ferry, C., An improved model to evaluate the oxidation kinetics of uranium dioxide during dry storage. *J. Nucl. Mater.*, 2007, **367**, 402–410.
4. McEachern, R. J., Choi, J. W., Kolar, M., Long, W., Taylor, P. and Wood, D. D., Determination of the activation energy for the formation of U_3O_8 on UO_2. *J. Nucl. Mater.*, 1997, **249**, 58–69.
5. Walker, D. E. Y., The oxidation of uranium dioxides. *J. Appl. Chem.*, 1965, **15**, 128–135.
6. Boase, D. G. and Vandergraaf, T. T., The Canadian spent fuel storage canister: some materials aspects. *Nucl. Technol.*, 1977, **32**, 60.
7. Valdivieso, F., Francon, V., Byasson, F., Pijolat, M., Feugier, A. and Peres, V., Oxidation behaviour of unirradiated sintered UO_2 pellets and powder at different oxygen partial pressures above 350 °C. *J. Nucl. Mater.*, 2006, **354**, 85–93.
8. Bae, K. K., Kim, B. G., Lee, Y. W., Yang and Park, H. S., Oxidation behaviour of unirradiated UO_2 pellets. *J. Nucl. Mater.*, 1994, **209**, 274–279.
9. Aronson, S., Roof Jr., R. B. and Belle, J., Kinetic study of the oxidation of uranium oxide. *J. Chem. Phys.*, 1957, **27**, 137.
10. Lefort, P., Demaison, J. and Billy, M., Comportement du nitrure cubique δ en atmosphère d'oxygène. *Mater. Res. Bull.*, 1979, **14**, 479–486.
11. Allen, G. C. and Tempest, P. A., Ordered defects in the oxides of uranium. *Proc. Roy. Soc. Lond. A*, 1986, **406**, 325–344.
12. Rousseau, G., Desgranges, L., Charlot, F., Millot, N., Niepce, J. C., Pijolat, M. *et al.*, A detailed study of UO_2 to U_3O_8 oxidation phases and the associated rate limiting steps. *J. Nucl. Mater.*, 2006, **355**, 10–20.
13. Pijolat, M. and Soustelle, M., Experimental tests to validate the rate-limiting step assumption used in the kinetic analysis of solid state reactions. *Thermochim. Acta*, 2008, **478**, 34–40.
14. Pijolat, M. and Soustelle, M., Experimental test to validate the rate equation "$d\alpha/dt = kf(\alpha)$" used in the kinetic analysis of solid state reactions. *Thermochim. Acta*, 2005, **439**, 86–93.
15. Higgs, J. D., Thompson, W. T., Lewis, B. J. and Vogel, S. C., Kinetics of precipitation of U_4O_9 from hyperstoichiometric UO_{2+x}. *J. Nucl. Mater.*, 2007, **366**, 297–305.
16. Dodé, M. and Touzelin, B., Etude directe aux rayons X en atmosphère contrôlée des équilibres d'oxydation des oxydes d'uranium de 1150 à 1200 °C. *Revue de Chimie Minérale*, 1972, **9**, 141–152.
17. Taylor, P., McEachern, R. J., Doern, D. C. and Wood, D. D., The influence of specimen roughness on the rate of formation of U_3O_8 on UO_2 in air at 250 °C. *J. Nucl. Mater.*, 1998, **256**, 213–217.